Efficient and stable solution-processed planar perovskite solar cells via contact passivation

Hairen Tan,[1] Ankit Jain,[1] Oleksandr Voznyy,[1] Xinzheng Lan,[1] F. Pelayo García de Arquer,[1] James Z. Fan,[1] Rafael Quintero-Bermudez,[1] Mingjian Yuan,[1] Bo Zhang,[1] Yicheng Zhao,[1] Fengjia Fan,[1] Peicheng Li,[2] Li Na Quan,[1] Yongbiao Zhao,[2] Zheng-Hong Lu,[2] Zhenyu Yang,[1] Sjoerd Hoogland,[1] Edward H. Sargent[1]*

[1]Department of Electrical and Computer Engineering, University of Toronto, 35 St George Street, Toronto, Ontario M5S 1A4, Canada. [2]Department of Materials Science and Engineering, University of Toronto, 184 College Street, Toronto, Ontario M5S 3E4, Canada.

*Corresponding author. Email: ted.sargent@utoronto.ca

Planar perovskite solar cells made entirely via solution-processing at low temperatures (<150°C) offer promise for simple manufacturing, compatibility with flexible substrates, and perovskite-based tandem devices; however, they require an electron-selective layer that performs well with similar processing. We report a contact passivation strategy using chlorine-capped TiO$_2$ colloidal nanocrystal (NC) film that mitigates interfacial recombination and improves interface binding in low-temperature planar solar cells. We fabricated solar cells with certified efficiencies of 20.1% and 19.5% for active areas of 0.049 and 1.1 square centimeters, respectively, achieved via low-temperature solution processing. Solar cells with efficiency >20% retained 90% (97% after dark recovery) of their initial performance after 500 hours continuous room-temperature operation at their maximum power point under one-sun illumination.

Metal halide perovskite solar cells (PSCs) have attracted extensive research interest for next-generation solution-processed photovoltaic (PV) devices because of their high solar-to-electric power conversion efficiency (PCE) and low fabrication cost (*1–4*). The top-performing PSCs, which have reached a certified PCE of 22.1%, have relied on high-temperature-sintered (450°C to 550°C) mesoporous TiO$_2$ as electron-selective layer (ESL) (*5–7*). However, this high-temperature processing makes manufacture more complex and hampers the development of flexible modules and perovskite-based monolithic tandem devices. To overcome this limitation, researchers have pursued planar PSCs that exploit low-temperature (typically < 150°C) solution-processed charge selective layers. Metal oxide materials such as TiO$_2$, ZnO, SnO$_2$, and Zn$_2$SnO$_4$ colloidal nanoparticles synthesized at low temperatures have commonly been used as the ESL (*8–16*). Very recently, high-efficiency (certified 19.9%), small-area PSCs have been achieved using low-temperature processed SnO$_2$ (*17, 18*).

Unfortunately, long-term device operational stability has remained far inferior to that of counterpart devices made using high-temperature-processed ESLs (*19–22*). Furthermore, PSCs having both high efficiency and large area, required for industrialization, have yet to be demonstrated in low-temperature planar PSCs (best large-area device uncertified PCE of 14.5% for PSCs using low-temperature-processed ESL; best large-area device certified PCE of 19.7%; however, these relied on high-temperature-sintered mesoporous TiO$_2$) (*23–25*).

We reasoned that performance and stability loss in low-temperature planar PSCs could arise from imperfect interfaces and charge recombination between the selective contact at the illumination side and the perovskite film grown on top (*4, 26, 27*), since the perovskite active layers themselves have excellent long-term photostability upon addition of formamidinium (FA), Cs, and Br ions (*19–22, 28*). Indeed, once the impressively long photocarrier diffusion lengths in perovskite films are achieved, attention must shift to perfecting the interface (*29–32*). We reasoned that deep trap states present at the perovskite/ESL interface could potentially be addressed by passivating the interface between the charge selective contact and the perovskite absorber.

Here we devise a simple and effective interface passivation method that leads to efficient and stable low-temperature-processed planar PSCs. Chlorine-capped TiO$_2$ colloidal nanocrystal (NC) films processed < 150°C were used as the ESL. The chloride additive in perovskite precursor solutions enhances grain-boundary passivation in MAPbI$_{3-x}$Cl$_x$ (MA, methylammonium cation, CH$_3$NH$_3^+$) PSCs (*33–36*). Here we find that the interfacial Cl atoms on the TiO$_2$ NCs suppress deep trap states at the perovskite interface and thus considerably reduce interface recombination at TiO$_2$/perovskite contact. The interfacial Cl atoms also lead to strong electronic coupling and chemical binding at the TiO$_2$/perovskite planar junction, as projected in previous theoretical studies (*37*). As a result, we fabricated hysteresis-free planar PSCs with independently-certified PCEs of 20.1% for small-area devices (0.049 cm^2) and 19.5% for large-area

devices (1.1 cm^2). The low-temperature planar PSCs with high initial PCE >20% exhibit excellent operational stability and retain 90% (97% after dark recovery) of their initial performance after 500 hours operating at their maximum power point under constant one-sun illumination.

We first examined defect passivation and interface binding by interfacial chlorine at the TiO$_2$/perovskite interface using density functional theory (DFT) (Fig. 1, fig. S1, and table S1) (*38*). We found that Cl at the interface results in stronger binding at the TiO$_2$/perovskite interface both for the cases of MAX- and PbX$_2$-terminated (X = Cl, I) perovskite surfaces. Perovskite films with the PbX$_2$-terminated interface are energetically favored to contact the TiO$_2$. Previous studies (*39–41*) have shown that, in bulk perovskites, the most detrimental defects (deep level defects) are antisites, but that their formation energy is relatively high, explaining the low trap-state density in MAPbI$_3$ perovskite films and single crystals. Vacancies and interstitials, although much more abundant, are shallow defects. We thus explored the effect of Cl at the interface on both antisite and vacancy defects. Without Cl, a Pb-I antisite defect leads to localized states near the valence band edge (Fig. 1A). They can capture holes and become non-radiative recombination centers. In contrast, the formation energy of the Pb-Cl antisite at the PbCl$_2$-terminated interface is higher (less favorable to form), indicating that antisite defects are suppressed in the presence of interfacial Cl atoms. The Pb-Cl antisite defect becomes much shallower and more delocalized (Fig. 1B) and has little effect on interface recombination. Overall, the incorporation of Cl atoms at the TiO$_2$/perovskite interface resulted in a lower density of interfacial trap states (fig. S1, B and D) as well as stronger binding between TiO$_2$ and perovskite (table S1).

We devised a synthetic approach to obtain Cl-capped TiO$_2$ NCs as the electron-selective layer in solar cells. We first synthesized anatase TiO$_2$ NCs of size ~5 nm (fig. S2) (*38*) via a nonhydrolytic method through the reaction of TiCl$_4$ and benzyl alcohol at 85°C under ambient atmosphere (*42*, *43*). This process results in Cl-capped TiO$_2$ NCs (TiO$_2$-Cl) with 12 ± 2 at.% of Cl relative to Ti atoms as determined using x-ray photoelectron spectroscopy (XPS, Fig. 1C). A mixture of methanol and chloroform was used to disperse the NCs while preserving surface Cl-ligands. XPS confirmed that surface Cl-ligands were well-retained after we formed films from a methanol-chloroform cosolvent (Fig. 1C). In contrast, the surface Cl-ligands were detached from TiO$_2$ surfaces when the washed NCs were redispersed in ethanol with a stabilizer such as titanium diisopropoxide bis(acetylacetonate) (TiAcAc). Such TiO$_2$ NCs that lack Cl-ligands – the ESL materials used in previous reports (*8*, *9*) – were taken as controls in the present study. Below, we denote the TiO$_2$ ESL with Cl-ligands as TiO$_2$-Cl; and the TiO$_2$

ESL lacking the Cl-ligands as TiO$_2$. The Cl atoms were strongly bound to TiO$_2$, and the Cl-ligands of TiO$_2$ thin film were retained on the surface after annealing up to 250°C (Fig. 1D).

We fabricated planar PSCs with TiO$_2$ as ESL with the device architecture of Fig. 2A. The TiO$_2$-Cl film on ITO-coated glass obtained by spin-coating was smooth and pinhole-free (Fig. 2B and fig. S3A). The film also exhibited negligible parasitic absorption loss over the entire visible to near-infrared spectral range (fig. S3B). Post-annealing at moderate temperatures was applied to improve the quality of the spin-cast TiO$_2$-Cl film. The best PV performance was achieved with a TiO$_2$-Cl annealing temperature of 150°C (table S2 and fig. S4). The mixed cation/halide perovskite layer FA$_{0.85}$MA$_{0.15}$PbI$_{2.55}$Br$_{0.45}$, with a thickness of ~600 nm, was deposited on the TiO$_2$-Cl film using the anti-solvent method (*38*, *44*, *45*). The processing solvent for perovskite precursors (e.g., dimethylsulfoxide, DMSO) did not remove surface Cl-ligands from the TiO$_2$-Cl film (fig. S5).

The bulk quality of perovskite films was similar on both TiO$_2$-Cl and TiO$_2$, a consequence of their identical processing. Smooth pinhole-free perovskite films with uniform and large grains were formed on both TiO$_2$-Cl and TiO$_2$ (Fig. 2C and fig. S6). As expected from the stoichiometric ratio of the precursors, x-ray diffraction (XRD) spectra show no obvious PbI$_2$ nor other non-perovskite phases in films (Fig. 2D). The sharp absorption edge and narrow PL spectrum of the perovskite film confirm a homogenous and single-phase material (fig. S7). The perovskite films on both TiO$_2$-Cl and TiO$_2$ exhibit a remarkably low trap state density of ~3 × 10^{15} cm^{-3} as determined using the space-charge limit current (SCLC) method (fig. S8). The band alignment between TiO$_2$-Cl (TiO$_2$) and perovskite was determined from ultraviolet photoelectron spectroscopy (UPS) and absorption measurements (fig. S9). The excellent match in conduction band minimum (CBM) between TiO$_2$-Cl and perovskite allowed efficient electron transfer into TiO$_2$-Cl, while the high offset in valence band maximum (VBM) provided efficient hole blocking.

We studied the charge transfer kinetics between perovskite and ESL using steady-state and time-resolved photoluminescence (TR-PL) spectroscopy. When perovskite films were formed on TiO$_2$ and TiO$_2$-Cl, the steady-state PL was quenched because of fast electron transfer to ESLs (Fig. 2E). Figure 2F shows the PL decays of the perovskite films on bare glass and on the TiO$_2$ and TiO$_2$-Cl coated ITO glass substrates. Table S3 summarizes the decays fit for biexponential components, a fast decay lifetime τ_1, and a slow decay lifetime τ_2. The perovskite film on bare glass showed a long lifetime (τ_2) of 470 ns. The PL lifetimes of perovskite films on ESLs were shortened to a similar degree for both TiO$_2$ and TiO$_2$-Cl. This result indicates that both ESLs had

sufficient electron extraction in solar cells, consistent with the good band alignments between the ESLs and perovskite.

To explore the effect of interfacial Cl atoms on the PV performance of planar PSCs, we made devices on the TiO_2-Cl and control TiO_2 ESLs. Figure S10 presents the statistical performance of 40 devices fabricated with otherwise-identical device processing on each type of ESL. Solar cells fabricated on TiO_2-Cl exhibit considerably better performance than those on TiO_2 for all PV metrics: the average V_{oc} increased from 1.06 V to 1.14 V with the incorporation of Cl; and the average FF increased from 69% to 77%. Correspondingly, TiO_2-Cl resulted in a higher average PCE (19.8%) than the Cl-free TiO_2 (15.8%).

Device performance measured after optimization is shown in Fig. 3A and table S4. These results confirm that the interfacial Cl-atoms, not the bulk properties of TiO_2 ESLs, dominate the performance of these perovskite solar cells. Figure 3B shows a histogram of PCE values over 200 planar PSCs fabricated on TiO_2-Cl within a period of 3 months. Excellent reproducibility is indicated by the narrow distribution of PCE values. The best-performing devices with TiO_2-Cl reached a PCE of 20.9%. The PCE from J-V sweeps is consistent with the stabilized maximum power output (fig. S11). The EQE spectrum (fig. S12) exhibited a broad plateau above 80% over the spectral range from 400 to 760 nm because of strong light harvesting within the thick perovskite film. Integration of the EQE curve with the AM1.5G solar spectrum yielded a photocurrent density of 22.6 mA cm^{-2}, in good agreement with the J_{sc} value from J-V characterization. We also examined the hysteresis of solar cells made on TiO_2-Cl and TiO_2 (Fig. 3A and table S4). Devices on TiO_2-Cl showed negligible hysteresis, while devices made on TiO_2 exhibit strong hysteresis, similar to previous reports using low-temperature TiO_2 as ETL (8, 9). The PV parameters of the Cl-free devices varied substantially with respect to scan direction.

To gain further insight into the performance enhancement resulting from the use of TiO_2-Cl, we characterized perovskite film properties, charge transfer kinetics, and charge recombination in solar cells with TiO_2 and TiO_2-Cl. The bulk quality of perovskite films and charge transfer were similar on both ESLs. Transient photocurrent decay under short-circuit conditions was obtained to study the influence of the ESL on charge transfer in solar cells (Fig. 3C). Cells with the two ESLs had comparable charge transport lifetime ($\tau_t \sim$ 3.4 μs), indicating similar interfacial charge transfer. This similarity indicates that either bulk quality or interface charge transfer is not the main reason for the solar cell performance enhancement by TiO_2-Cl.

We characterized solar cells using transient photovoltage decay under the open-circuit condition and found that the charge recombination lifetime (τ_r) of the device on TiO_2-Cl

was substantially longer than that of the device on TiO_2 (145 μs versus 64 μs; Fig. 3D), consistent with slowed charge recombination at the TiO_2-Cl/perovskite interface. The reduced ideality factor of solar cells with TiO_2-Cl (n = 1.25) compared to TiO_2 (n = 1.73) is consistent with suppressed interfacial recombination (fig. S13). As seen in the DFT studies, interfacial Cl atoms suppress the formation of deep trap states on the surface of perovskite films, leading to improved surface passivation and reduced interfacial recombination.

To examine the applicability of TiO_2-Cl to other high-efficiency PSCs, we fabricated devices using cesium-containing perovskite $Cs_{0.05}FA_{0.81}MA_{0.14}PbI_{2.55}Br_{0.45}$ (denoted as CsMAFA), which had been shown to improve performance and photostability compared to $FA_{0.85}MA_{0.15}PbI_{2.55}Br_{0.45}$ (denoted as MAFA) (22, 46, 47). The best-performing small-area CsMAFA solar cell (0.049 cm^2) exhibited a high laboratory PCE of 21.4% (V_{oc} = 1.189 V, J_{sc} = 22.3 mA/cm^2, FF = 0.806) without hysteresis in J-V sweeps (Fig. 3E). We also fabricated large-area (1.1 cm^2) CsMAFA solar cells on TiO_2-Cl, showing a PCE value >20% with negligible hysteresis (Fig. 3F). A small-area and a large-area device were sent, without encapsulation, to an accredited independent PV test laboratory (Newport Corporation PV Lab, MT, USA) for certification. They gave certified PCEs of 20.1% and 19.5%, respectively (figs. S14 to S16). The large-area device exhibited ~3% performance loss relative to the small-area device. The certified PCE of 19.5% for large-area, low-temperature planar PSC exceeds that of other reported low-temperature or planar PSCs (24, 25), and it approaches the certified PCE of large-area cells that relied on high-temperature-sintered mesoporous TiO_2 (table S5) (23, 38, 48).

We examined the long-term stability of low-temperature planar PSCs made on TiO_2-Cl and TiO_2 under dark storage as well as under operating conditions. The long-term stability of PSCs is closely related to the front ESL/perovskite interface binding strength and interfacial charge accumulation during operation (49, 50). The devices made on TiO_2-Cl showed substantially enhanced stability relative to TiO_2 under dark storage (Fig. 4A). MAFA based devices on TiO_2-Cl maintained 95% of their initial PCE after storage in the dark over 60 days, while those on TiO_2 only retained 38% of their initial efficiency (Fig. 4A). The high-efficiency CsMAFA devices on TiO_2-Cl (initial PCE>21%) exhibited promising shelf stability, retaining 96% of their initial performance after 90 days (over 2,000 hours).

Solar cells must operate stably under maximum power point (MPP) conditions. The MAFA solar cells based on TiO_2-Cl showed improved stability under continuous operation at MPP compared to devices based on TiO_2 (fig. S17). Impressively, the CsMAFA solar cell on TiO_2-Cl (with 420-

nm cutoff UV filter) retained 90% of their initial performance after continuous operation for 500 hours under one-sun illumination, as directly determined from the MPP tracking (Fig. 4B). The PCE increased slightly in the first tens of hours of MPP operation, which may be caused by light-induced defect healing in the perovskite active layer (*19*, *51*). No perovskite decomposition was observed after MPP operation as seen from XRD (fig. S18), indicating that the performance drop during MPP operation may be caused by defect generation in the perovskite layer (*52*, *53*) and changes to the perovskite/Spiro-OMeTAD interface (the latter has previously been shown to be vulnerable) (*54*–*56*). The device self-recovered to an efficiency of 19.8% (97% of initial PCE) following dark storage (Fig. 4C), consistent with previous reports (*18*, *19*, *52*).

Overall, the stronger binding at the TiO_2-Cl/perovskite interface and the suppressed interfacial recombination account for superior stability in planar PSCs based on TiO_2-Cl. The new approach to fabricate efficient and stable perovskite solar cells is simple and scalable, compatible with future industrialization of perovskite-based PV technology. It offers a promising path to flexible devices and to combining with low-band-gap semiconductor materials to form tandem devices.

REFERENCES AND NOTES

1. S. D. Stranks, H. J. Snaith, Metal-halide perovskites for photovoltaic and light-emitting devices. *Nat. Nanotechnol.* **10**, 391–402 (2015). doi:10.1038/nnano.2015.90 Medline

2. M. A. Green, A. Ho-Baillie, H. J. Snaith, The emergence of perovskite solar cells. *Nat. Photonics* **8**, 506–514 (2014). doi:10.1038/nphoton.2014.134

3. Y. Zhao, K. Zhu, Organic-inorganic hybrid lead halide perovskites for optoelectronic and electronic applications. *Chem. Soc. Rev.* **45**, 655–689 (2016). doi:10.1039/C4CS00458B Medline

4. N. Park, M. Grätzel, T. Miyasaka, K. Zhu, K. Emery, Towards stable and commercially available perovskite solar cells. *Nat. Energy* **1**, 16152 (2016). doi:10.1038/nenergy.2016.152

5. W. S. Yang, J. H. Noh, N. J. Jeon, Y. C. Kim, S. Ryu, J. Seo, S. I. Seok, High-performance photovoltaic perovskite layers fabricated through intramolecular exchange. *Science* **348**, 1234–1237 (2015). doi:10.1126/science.aaa9272 Medline

6. D. Bi, C. Yi, J. Luo, J.-D. Décoppet, F. Zhang, S. M. Zakeeruddin, X. Li, A. Hagfeldt, M. Grätzel, Polymer-templated nucleation and crystal growth of perovskite films for solar cells with efficiency greater than 21%. *Nat. Energy* **1**, 16142 (2016). doi:10.1038/nenergy.2016.142

7. D.-Y. Son, J.-W. Lee, Y. J. Choi, I.-H. Jang, S. Lee, P. J. Yoo, H. Shin, N. Ahn, M. Choi, D. Kim, N.-G. Park, Self-formed grain boundary healing layer for highly efficient $CH_3NH_3PbI_3$ perovskite solar cells. *Nat. Energy* **1**, 16081 (2016). doi:10.1038/nenergy.2016.81

8. H. Zhou, Q. Chen, G. Li, S. Luo, T. B. Song, H.-S. Duan, Z. Hong, J. You, Y. Liu, Y. Yang, Interface engineering of highly efficient perovskite solar cells. *Science* **345**, 542–546 (2014). doi:10.1126/science.1254050 Medline

9. K. Wojciechowski, M. Saliba, T. Leijtens, A. Abate, H. J. Snaith, Sub-150°C processed meso-superstructured perovskite solar cells with enhanced efficiency. *Energy Environ. Sci.* **7**, 1142–1147 (2014). doi:10.1039/C3EE43707H

10. S. S. Shin, W. S. Yang, J. H. Noh, J. H. Suk, N. J. Jeon, J. H. Park, J. S. Kim, W. M. Seong, S. I. Seok, High-performance flexible perovskite solar cells exploiting Zn_2SnO_4 prepared in solution below 100°C. *Nat. Commun.* **6**, 7410 (2015). doi:10.1038/ncomms8410 Medline

11. D. Liu, T. L. Kelly, Perovskite solar cells with a planar heterojunction structure prepared using room-temperature solution processing techniques. *Nat. Photonics* **8**, 133–138 (2013). doi:10.1038/nphoton.2013.342

12. J. You, L. Meng, T.-B. Song, T.-F. Guo, Y. M. Yang, W.-H. Chang, Z. Hong, H. Chen, H. Zhou, Q. Chen, Y. Liu, N. De Marco, Y. Yang, Improved air stability of perovskite solar cells via solution-processed metal oxide transport layers. *Nat. Nanotechnol.* **11**, 75–81 (2016). doi:10.1038/nnano.2015.230 Medline

13. X. Liu, K.-W. Tsai, Z. Zhu, Y. Sun, C.-C. Chueh, A. K.-Y. Jen, A low-temperature, solution processable tin oxide electron-transporting layer prepared by the dual-fuel combustion method for efficient perovskite solar cells. *Adv. Mater. Interfaces* **3**, 1600122 (2016). doi:10.1002/admi.201600122

14. Z. Zhu, Y. Bai, X. Liu, C.-C. Chueh, S. Yang, A. K.-Y. Jen, Enhanced efficiency and stability of inverted perovskite solar cells using highly crystalline SnO_2 nanocrystals as the robust electron-transporting layer. *Adv. Mater.* **28**, 6478–6484 (2016). doi:10.1002/adma.201600619 Medline

15. T. A. Berhe, W.-N. Su, C.-H. Chen, C.-J. Pan, J.-H. Cheng, H.-M. Chen, M.-C. Tsai, L.-Y. Chen, A. A. Dubale, B.-J. Hwang, Organometal halide perovskite solar cells: Degradation and stability. *Energy Environ. Sci.* **9**, 323–356 (2016). doi:10.1039/C5EE02733K

16. H. Kim, K.-G. Lim, T.-W. Lee, Planar heterojunction organometal halide perovskite solar cells: Roles of interfacial layers. *Energy Environ. Sci.* **9**, 12–30 (2016). doi:10.1039/C5EE02194D

17. Q. Jiang, L. Zhang, H. Wang, X. Yang, J. Meng, H. Liu, Z. Yin, J. Wu, X. Zhang, J. You, Enhanced electron extraction using SnO_2 for high-efficiency planar-structure $HC(NH_2)_2PbI_3$-based perovskite solar cells. *Nat. Energy* **2**, 16177 (2016). doi:10.1038/nenergy.2016.177

18. E. H. Anaraki, A. Kermanpur, L. Steier, K. Domanski, T. Matsui, W. Tress, M. Saliba, A. Abate, M. Grätzel, A. Hagfeldt, J.-P. Correa-Baena, Highly efficient and stable planar perovskite solar cells by solution-processed tin oxide. *Energy Environ. Sci.* **9**, 3128–3134 (2016). doi:10.1039/C6EE02390H

19. M. Saliba, T. Matsui, K. Domanski, J.-Y. Seo, A. Ummadisingu, S. M. Zakeeruddin, J.-P. Correa-Baena, W. R. Tress, A. Abate, A. Hagfeldt, M. Grätzel, Incorporation of rubidium cations into perovskite solar cells improves photovoltaic performance. *Science* **354**, 206–209 (2016). doi:10.1126/science.aah5557 Medline

20. W. Chen, Y. Wu, Y. Yue, J. Liu, W. Zhang, X. Yang, H. Chen, E. Bi, I. Ashraful, M. Grätzel, L. Han, Efficient and stable large-area perovskite solar cells with inorganic charge extraction layers. *Science* **350**, 944–948 (2015). doi:10.1126/science.aad1015 Medline

21. A. Mei, X. Li, L. Liu, Z. Ku, T. Liu, Y. Rong, M. Xu, M. Hu, J. Chen, Y. Yang, M. Grätzel, H. Han, A hole-conductor-free, fully printable mesoscopic perovskite solar cell with high stability. *Science* **345**, 295–298 (2014). doi:10.1126/science.1254763 Medline

22. M. Saliba, T. Matsui, J.-Y. Seo, K. Domanski, J.-P. Correa-Baena, M. K. Nazeeruddin, S. M. Zakeeruddin, W. Tress, A. Abate, A. Hagfeldt, M. Grätzel, Cesium-containing triple cation perovskite solar cells: Improved stability, reproducibility and high efficiency. *Energy Environ. Sci.* **9**, 1989–1997 (2016). doi:10.1039/C5EE03874J Medline

23. X. Li, D. Bi, C. Yi, J.-D. Décoppet, J. Luo, S. M. Zakeeruddin, A. Hagfeldt, M. Grätzel, A vacuum flash-assisted solution process for high-efficiency large-area perovskite solar cells. *Science* **353**, 58–62 (2016). doi:10.1126/science.aaf8060 Medline

24. Y. Wu, X. Yang, W. Chen, Y. Yue, M. Cai, F. Xie, E. Bi, A. Islam, L. Han, Perovskite solar cells with 18.21% efficiency and area over 1 cm^2 fabricated by heterojunction engineering. *Nat. Energy* **1**, 16148 (2016). doi:10.1038/nenergy.2016.148

25. J. Werner, L. Barraud, A. Walter, M. Bräuninger, F. Sahli, D. Sacchetto, N. Tétreault, B. Paviet-Salomon, S.-J. Moon, C. Allebé, M. Despeisse, S. Nicolay, S. De Wolf, B. Niesen, C. Ballif, Efficient near-infrared-transparent perovskite solar cells enabling direct comparison of 4-terminal and monolithic perovskite/silicon tandem cells. *ACS Energy Lett.* **1**, 474–480 (2016). doi:10.1021/acsenergylett.6b00254

26. T. Singh, J. Singh, T. Miyasaka, Role of metal oxide electron-transport layer modification on the stability of high performing perovskite solar cells. *ChemSusChem* **9**, 2559–2566 (2016). doi:10.1002/cssc.201601004 Medline

27. N. Ahn, K. Kwak, M. S. Jang, H. Yoon, B. Y. Lee, J.-K. Lee, P. V. Pikhitsa, J. Byun,

M. Choi, Trapped charge-driven degradation of perovskite solar cells. *Nat. Commun.* **7**, 13422 (2016). doi:10.1038/ncomms13422 Medline

28. H. Tsai, W. Nie, J.-C. Blancon, C. C. Stoumpos, R. Asadpour, B. Harutyunyan, A. J. Neukirch, R. Verduzco, J. J. Crochet, S. Tretiak, L. Pedesseau, J. Even, M. A. Alam, G. Gupta, J. Lou, P. M. Ajayan, M. J. Bedzyk, M. G. Kanatzidis, A. D. Mohite, High-efficiency two-dimensional Ruddlesden-Popper perovskite solar cells. *Nature* **536**, 312–316 (2016). doi:10.1038/nature18306 Medline

29. Y. Shao, Y. Yuan, J. Huang, Correlation of energy disorder and open-circuit voltage in hybrid perovskite solar cells. *Nat. Energy* **1**, 15001 (2016). doi:10.1038/nenergy.2015.1

30. Q. Wang, Q. Dong, T. Li, A. Gruverman, J. Huang, Thin insulating tunneling contacts for efficient and water-resistant perovskite solar cells. *Adv. Mater.* **28**, 6734–6739 (2016). doi:10.1002/adma.201600969 Medline

31. Y. Li, Y. Zhao, Q. Chen, Y. M. Yang, Y. Liu, Z. Hong, Z. Liu, Y.-T. Hsieh, L. Meng, Y. Li, Y. Yang, Multifunctional fullerene derivative for interface engineering in perovskite solar cells. *J. Am. Chem. Soc.* **137**, 15540–15547 (2015). doi:10.1021/jacs.5b10614 Medline

32. F. Giordano, A. Abate, J. P. Correa Baena, M. Saliba, T. Matsui, S. H. Im, S. M. Zakeeruddin, M. K. Nazeeruddin, A. Hagfeldt, M. Graetzel, Enhanced electronic properties in mesoporous TiO2 via lithium doping for high-efficiency perovskite solar cells. *Nat. Commun.* **7**, 10379 (2016). doi:10.1038/ncomms10379 Medline

33. D. W. de Quilettes, S. M. Vorpahl, S. D. Stranks, H. Nagaoka, G. E. Eperon, M. E. Ziffer, H. J. Snaith, D. S. Ginger, Impact of microstructure on local carrier lifetime in perovskite solar cells. *Science* **348**, 683–686 (2015). doi:10.1126/science.aaa5333 Medline

34. Q. Chen, H. Zhou, Y. Fang, A. Z. Stieg, T.-B. Song, H.-H. Wang, X. Xu, Y. Liu, S. Lu, J. You, P. Sun, J. McKay, M. S. Goorsky, Y. Yang, The optoelectronic role of chlorine in CH₃NH₃PbI₃(Cl)-based perovskite solar cells. *Nat. Commun.* **6**, 7269 (2015). doi:10.1038/ncomms8269 Medline

35. D. E. Starr, G. Sadoughi, E. Handick, R. G. Wilks, J. H. Alsmeier, L. Köhler, M. Gorgoi, H. J. Snaith, M. Bär, Direct observation of an inhomogeneous chlorine distribution in CH₃NH₃PbI₃₋ₓClₓ layers: Surface depletion and interface enrichment. *Energy Environ. Sci.* **8**, 1609–1615 (2015). doi:10.1039/C5EE00403A

36. J. Chae, Q. Dong, J. Huang, A. Centrone, Chloride incorporation process in CH₃NH₃PbI₃₋ₓClₓ perovskites via nanoscale bandgap maps. *Nano Lett.* **15**, 8114–8121 (2015). doi:10.1021/acs.nanolett.5b03556 Medline

37. E. Mosconi, E. Ronca, F. De Angelis, First-principles investigation of the TiO₂/organohalide perovskites interface: The role of interfacial chlorine. *J. Phys. Chem. Lett.* **5**, 2619–2625 (2014). doi:10.1021/jz501127k Medline

38. See supplementary materials.

39. W. Yin, T. Shi, Y. Yan, Unusual defect physics in CH₃NH₃PbI₃ perovskite solar cell absorber. *Appl. Phys. Lett.* **104**, 063903 (2014). doi:10.1063/1.4864778

40. A. Buin, P. Pietsch, J. Xu, O. Voznyy, A. H. Ip, R. Comin, E. H. Sargent, Materials processing routes to trap-free halide perovskites. *Nano Lett.* **14**, 6281–6286 (2014). doi:10.1021/nl502612m Medline

41. W. Yin, J. Yang, J. Kang, Y. Yan, S.-H. Wei, Halide perovskite materials for solar cells: A theoretical review. *J. Mater. Chem. A Mater. Energy Sustain.* **3**, 8926–8942 (2015). doi:10.1039/C4TA05033A

42. M. Niederberger, M. H. Bartl, G. D. Stucky, Benzyl alcohol and titanium tetrachloride – A versatile reaction system for the nonaqueous and low-temperature preparation of crystalline and luminescent titania nanoparticles. *Chem. Mater.* **14**, 4364–4370 (2002). doi:10.1021/cm021203k

43. J. Wang, J. Polleux, J. Lim, B. Dunn, Pseudocapacitive contributions to electrochemical energy storage in TiO₂ (anatase) nanoparticles. *J. Phys. Chem. C* **111**, 14925–14931 (2007). doi:10.1021/jp074464w

44. N. J. Jeon, J. H. Noh, Y. C. Kim, W. S. Yang, S. Ryu, S. I. Seok, Solvent engineering for high-performance inorganic-organic hybrid perovskite solar cells. *Nat. Mater.* **13**, 897–903 (2014). doi:10.1038/nmat4014 Medline

45. D. Bi, W. Tress, M. I. Dar, P. Gao, J. Luo, C. Renevier, K. Schenk, A. Abate, F. Giordano, J.-P. Correa Baena, J.-D. Decoppet, S. M. Zakeeruddin, M. K. Nazeeruddin, M. Grätzel, A. Hagfeldt, Efficient luminescent solar cells based on tailored mixed-cation perovskites. *Sci. Adv.* **2**, e1501170 (2016). doi:10.1126/sciadv.1501170 Medline

46. J.-W. Lee, D.-H. Kim, H.-S. Kim, S.-W. Seo, S. M. Cho, N.-G. Park, Formamidinium and cesium hybridization for photo- and moisture-stable perovskite solar cell. *Adv. Energy Mater.* **5**, 1501310 (2015). doi:10.1002/aenm.201501310

47. Z. Li, M. Yang, J.-S. Park, S.-H. Wei, J. J. Berry, K. Zhu, Stabilizing perovskite structures by tuning tolerance factor: Formation of formamidinium and cesium lead iodide solid-state alloys. *Chem. Mater.* **28**, 284–292 (2016). doi:10.1021/acs.chemmater.5b04107

48. M. A. Green, K. Emery, Y. Hishikawa, W. Warta, E. D. Dunlop, Solar cell efficiency tables (version 48). *Prog. Photovolt. Res. Appl.* **24**, 905–913 (2016). doi:10.1002/pip.2788

49. W. Tress, J. P. Correa Baena, M. Saliba, A. Abate, M. Graetzel, Inverted current-voltage hysteresis in mixed perovskite solar cells: Polarization, energy barriers, and defect recombination. *Adv. Energy Mater.* **6**, 1600396 (2016). doi:10.1002/aenm.201600396

50. Y. Yuan, J. Huang, Ion migration in organometal trihalide perovskite and its impact on photovoltaic efficiency and stability. *Acc. Chem. Res.* **49**, 286–293 (2016). doi:10.1021/acs.accounts.5b00420 Medline

51. E. Mosconi, D. Meggiolaro, H. J. Snaith, S. D. Stranks, F. De Angelis, Light-induced annihilation of Frenkel defects in organo-lead halide perovskites. *Energy Environ. Sci.* **9**, 3180–3187 (2016). doi:10.1039/C6EE01504B

52. W. Nie, J.-C. Blancon, A. J. Neukirch, K. Appavoo, H. Tsai, M. Chhowalla, M. A. Alam, M. Y. Sfeir, C. Katan, J. Even, S. Tretiak, J. J. Crochet, G. Gupta, A. D. Mohite, Light-activated photocurrent degradation and self-healing in perovskite solar cells. *Nat. Commun.* **7**, 11574 (2016). doi:10.1038/ncomms11574 Medline

53. D. W. deQuilettes, W. Zhang, V. M. Burlakov, D. J. Graham, T. Leijtens, A. Osherov, V. Bulović, H. J. Snaith, D. S. Ginger, S. D. Stranks, Photo-induced halide redistribution in organic-inorganic perovskite films. *Nat. Commun.* **7**, 11683 (2016). doi:10.1038/ncomms11683 Medline

54. K. Domanski, J.-P. Correa-Baena, N. Mine, M. K. Nazeeruddin, A. Abate, M. Saliba, W. Tress, A. Hagfeldt, M. Grätzel, Not all that glitters is gold: Metal-migration-induced degradation in perovskite solar cells. *ACS Nano* **10**, 6306–6314 (2016). doi:10.1021/acsnano.6b02613 Medline

55. A. Guerrero, J. You, C. Aranda, Y. S. Kang, G. Garcia-Belmonte, H. Zhou, J. Bisquert, Y. Yang, Interfacial degradation of planar lead halide perovskite solar cells. *ACS Nano* **10**, 218–224 (2016). doi:10.1021/acsnano.5b03687 Medline

56. Z. Hawash, L. K. Ono, S. R. Raga, M. V. Lee, Y. Qi, Air-exposure induced dopant redistribution and energy level shifts in spin-coated spiro-MeOTAD films. *Chem. Mater.* **27**, 562–569 (2015). doi:10.1021/cm504022q

57. J. P. Perdew, K. Burke, M. Ernzerhof, Generalized Gradient approximation made simple. *Phys. Rev. Lett.* **77**, 3865–3868 (1996). doi:10.1103/PhysRevLett.77.3865 Medline

58. J. VandeVondele, J. Hutter, Gaussian basis sets for accurate calculations on molecular systems in gas and condensed phases. *J. Chem. Phys.* **127**, 114105 (2007). doi:10.1063/1.2770708 Medline

59. H. Press et al., *The Art of Scientific Computing 3rd edition*, CH. 10.9 (Cambridge Univ. Press, 2007).
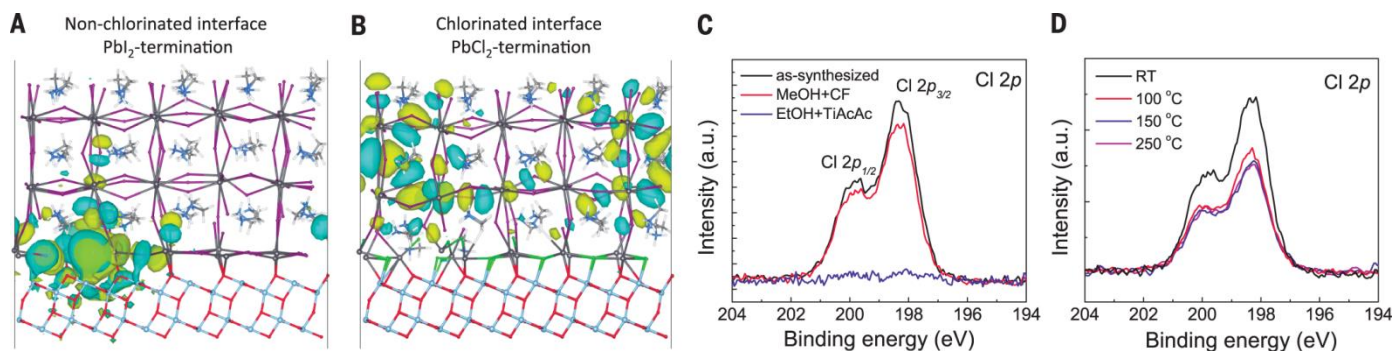
ACKNOWLEDGMENTS

Fig. 1. The effect of Cl on interface quality between perovskite and TiO$_2$, and stabilization of Cl-capped TiO$_2$ (TiO$_2$-Cl) colloidal nanocrystals. (A) Trap-like localized antisite defects form near the valence band edge for the PbI$_2$-terminated TiO$_2$/perovskite interface. (B) Shallow and delocalized Pb-Cl antisite defects are seen for the PbCl$_2$-terminated interface. (C and D) XPS spectra of Cl $2p$ peak of (C) TiO$_2$ NC films: as-synthesized, redispersed in the cosolvent of methanol and chloroform (MeOH + CF), redispersed in ethanol with titanium diisopropoxide bis(acetylacetonate) as stabilizer (EtOH + TiAcAc) and (D) TiO$_2$-Cl NC films with various post-annealing temperatures: room temperature (RT), 100°C, 150°C, and 250°C.
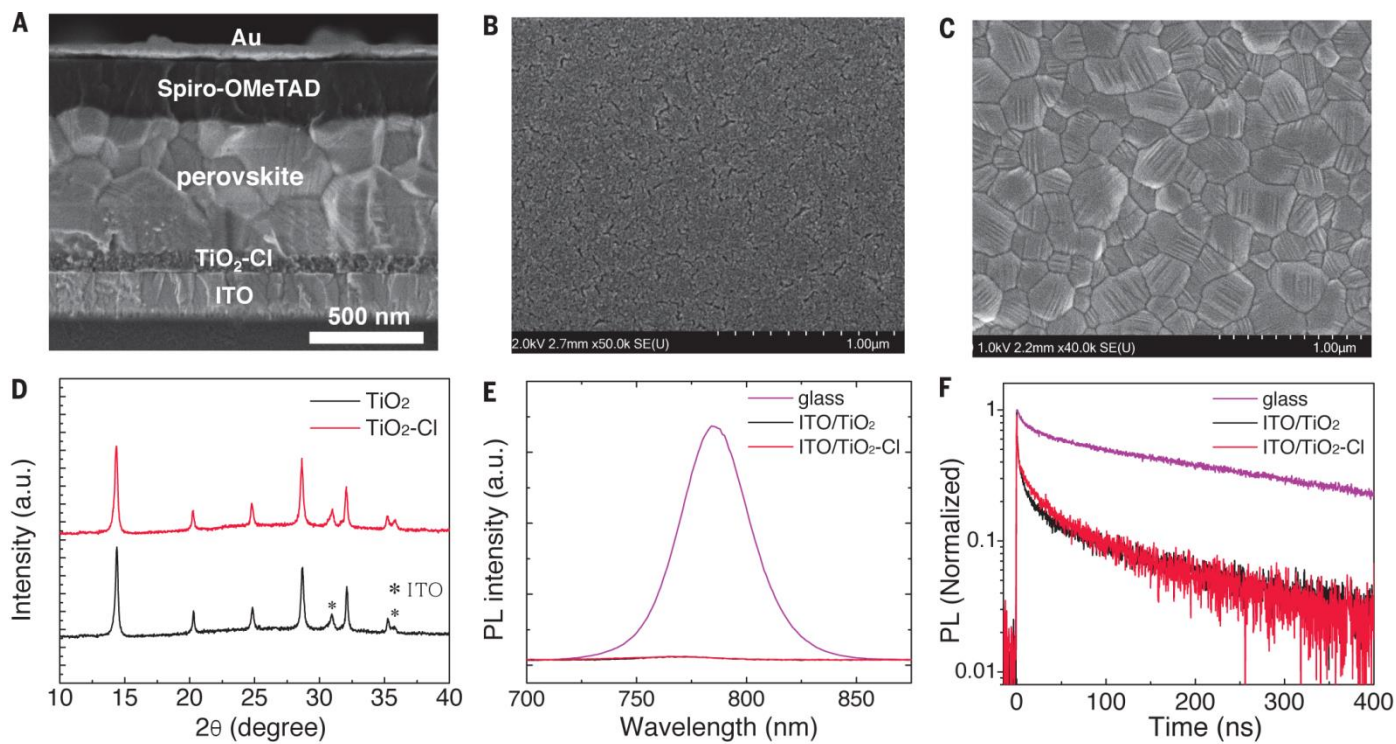
Fig. 2. Device structure and characterization of perovskite films on TiO₂-Cl. (A) Device structure and cross-sectional scanning electron microscopy (SEM) image of planar PSC. (B and C) Top-view SEM images of the TiO₂-Cl film on ITO substrate (B) and the perovskite film on TiO₂-Cl (C). (D) XRD patterns of perovskite films on TiO₂ and TiO₂-Cl. (E) Steady-state PL spectra and (F) time-resolved PL decays of perovskite films on bare glass, and on TiO₂ and TiO₂-Cl coated ITO substrates. The PL signals of perovskite films on TiO₂ and TiO₂-Cl were effectively quenched by the fast charge extraction by TiO₂ and TiO₂-Cl.
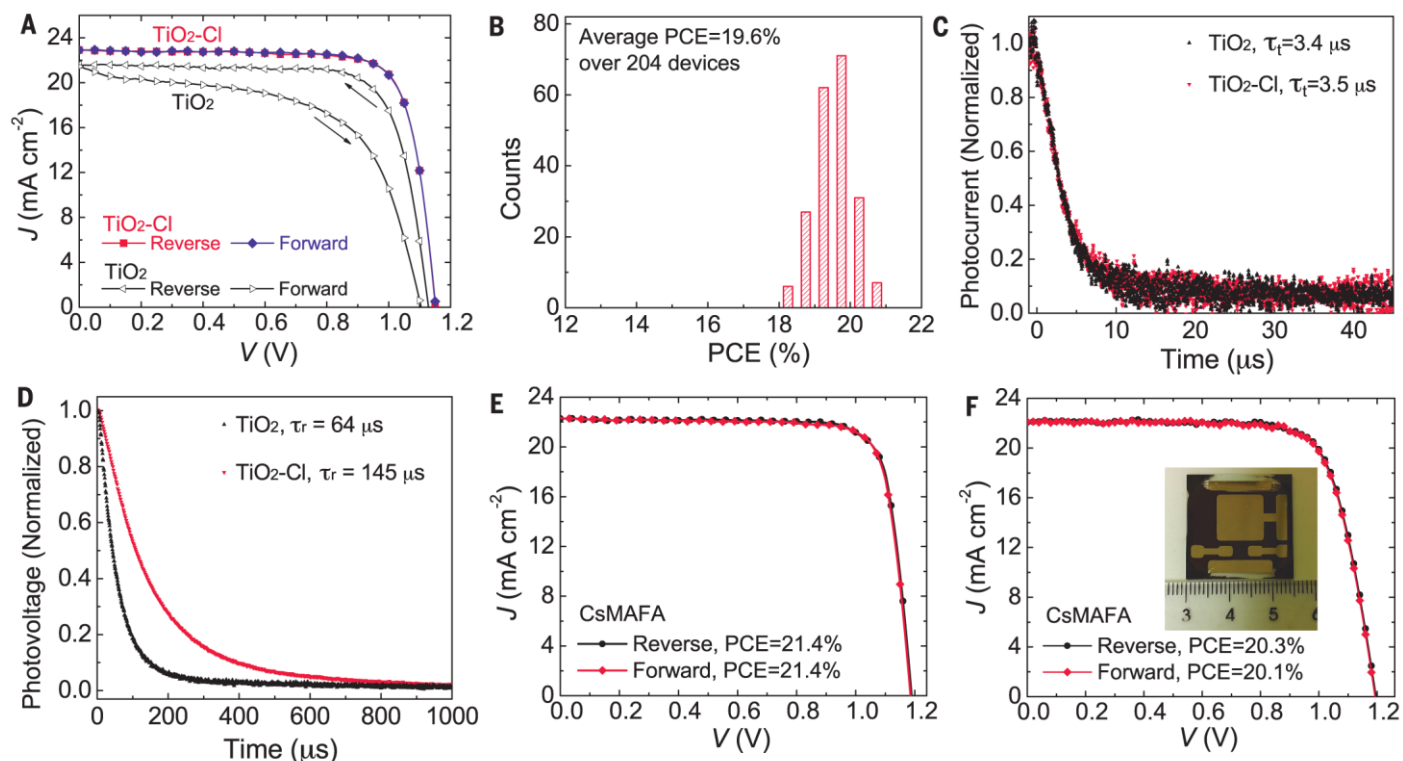
Fig. 3. Enhanced photovoltaic performance of perovskite solar cells with TiO$_2$-Cl. (A) *J-V* curves of PSCs with TiO$_2$ and TiO$_2$-Cl as ESLs measured at reverse and forward scans. (B) Histogram of the PCE values among 204 devices on TiO$_2$-Cl. (C) Normalized transient photocurrent decay and (D) normalized transient photovoltage decay of solar cells with TiO$_2$ and TiO$_2$-Cl as ESLs. Devices shown in A-D have perovskite composition of MAFA. (E) *J-V* curves of best-performing small-area (0.049 cm^2) CsMAFA PSC measured at reverse and forward scans. (F) *J-V* curves of best-performing large-area (1.1 cm^2) CsMAFA PSC showing a PCE of 20.3% (V_{oc} = 1.196 V, J_{sc} = 22.2 mA cm^{-2}, FF = 76.4%) at reverse scan. The inset shows the photo of the large-area device. MAFA and CsMAFA denote the perovskite compositions of FA$_{0.85}$MA$_{0.15}$PbI$_{2.55}$Br$_{0.45}$ and Cs$_{0.05}$FA$_{0.81}$MA$_{0.14}$PbI$_{2.55}$Br$_{0.45}$, respectively.
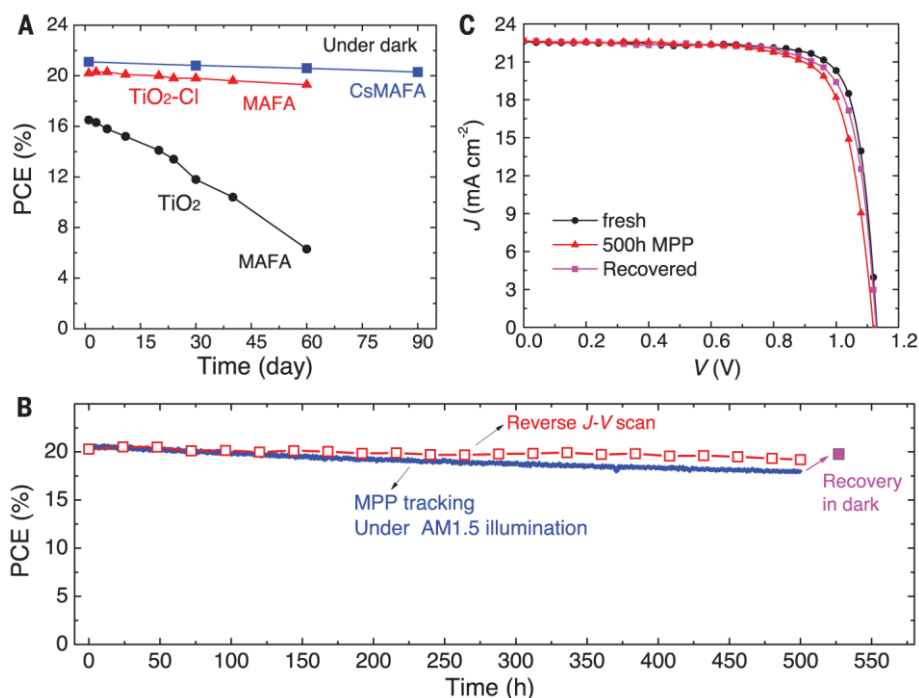
Fig. 4. Long-term device stability of perovskite solar cells with TiO$_2$-Cl and TiO$_2$. (**A**) Dark storage stability of non-encapsulated PSCs using TiO$_2$ and TiO$_2$-Cl. The unsealed cells were kept in a dry cabinet (<30% relative humidity) in the dark and measured regularly in nitrogen. PCE values were obtained from the reverse scans. MAFA and CsMAFA represent the perovskite compositions of FA$_{0.85}$MA$_{0.15}$PbI$_{2.55}$Br$_{0.45}$ and Cs$_{0.05}$FA$_{0.81}$MA$_{0.14}$PbI$_{2.55}$Br$_{0.45}$, respectively. (**B**) Continuous maximum power point (MPP) tracking for 500 hours of a high-performance unsealed CsMAFA cell with TiO$_2$-Cl in nitrogen atmosphere under constant simulated solar illumination (100 mW cm^{-2}) with a 420 nm cutoff UV filter. PCE values taken from reverse *J-V* scans (square symbols) are shown as well; the device retains 95% of initial performance as determined from reverse *J-V* scans. (**C**) *J-V* curves of PSC (CsMAFA) shown in (B) at various stages: fresh, right after 500 hours of MPP operation, and after recovery overnight in the dark. The *J-V* curves were measured without UV-filter

Editor's Summary

Article Tools   Visit the online version of this article to access the personalization and article tools:
http://science.sciencemag.org/content/early/2017/02/01/science.aai9081

Permissions   Obtain information about reproducing this article:
http://www.sciencemag.org/about/permissions.dtl